Fermi National Accelerator Laboratory

FERMILAB-PUB-90/189-T
MAD/PH/590
September 1990

Tagging the Higgs Boson in $pp \to W^+W^-jj$

U. Baur*

Physics Department, University of Wisconsin

Madison, WI 53706, USA

and

E. W. N. Glover*

Fermi National Accelerator Laboratory

P. O. Box 500, Batavia, IL 60510, USA

ABSTRACT

We compute the exact matrix elements for the tree level $\mathcal{O}(\alpha_W^4)$ process $qq \to qqW^+W^-$ and the tree level $\mathcal{O}(\alpha_s^2\alpha_W^2)$ mixed QCD-electroweak processes, $gg \to q\bar{q}W^+W^-$, *etc.* and use them to examine the Higgs boson signal in $pp \to W^+W^-jj$ for the representative case $m_H = 800$ GeV. By requiring two 'tagging' jets, $p_{Tj} > 50$ GeV and $2.5 < |\eta_j| < 5.0$ (4.5) at the SSC (LHC), the W^+W^-jj backgrounds from the mixed QCD-electroweak process and the non-resonant purely electroweak $qq \to qqW^+W^-$ process are significantly reduced. We find that the m_{WW} distribution of the Higgs boson signal is poorly described by the s-channel Higgs pole approximation.

---

* SSC Fellow

Operated by Universities Research Association Inc. under contract with the United States Department of Energy

One of the primary objectives of the SSC and LHC is the investigation of the electroweak symmetry breaking sector and the search for the Higgs boson. For heavy Higgs bosons, $m_H > 2M_Z$, the dominant decays are $H \to W^+W^-$ and $H \to ZZ$ so that the best place to look for evidence of the Higgs boson at hadron supercolliders is in $pp \to VVX$ where $V = W,\ Z$. There are two important production mechanisms for Higgs bosons in these channels. First, via gluon fusion, where the gluons couple to the Higgs boson via a top quark loop,[1-3]

$$gg \to H \to VV, \tag{1}$$

and second, via 'vector boson fusion',[4-6]

$$qq \to qqH \to qqVV. \tag{2}$$

In this case, the incoming partons emit electroweak bosons which annihilate into a Higgs boson. Due to the Yukawa coupling of the top quark with the Higgs boson, the gluon fusion cross section depends strongly on the top quark mass, and, for $m_t > 89$ GeV, the present lower limit,[7] dominates at the SSC provided $m_H \leq 600$ GeV. The vector boson fusion cross section becomes important for larger Higgs boson masses.

The cleanest channels to examine are the decays $H \to ZZ \to \ell^+\ell^-\ell'^+\ell'^-$ (with $\ell,\ \ell' = e,\ \mu$) and $H \to ZZ \to \ell^+\ell^-\nu\bar{\nu}$ which have branching ratios of 0.0014 and 0.0088 respectively. Current estimates using the exact matrix elements at the parton level suggest that a Higgs boson can be identified in these channels with an integrated luminosity of $\int \mathcal{L}\ dt = 10^4$ pb^{-1} provided $m_H \leq 600$ GeV at the LHC (pp collisions at $\sqrt{s} = 16$ TeV) and $m_H \leq 800$ GeV at the SSC (pp collisions at $\sqrt{s} = 40$ TeV).[8] For larger Higgs boson masses, the event rate is too small to observe a clear signal, and to extend the range of observability would require an increased data sample.

On the other hand, the semileptonic Higgs decay, $H \to W^+W^- \to \ell\nu q\bar{q}$, offers the possibility of exploiting the much larger branching ratio of ≈ 0.20. In this case, however, there is a sizeable background from $W+$ multijet production where two

of the QCD jets have an invariant mass close to M_W and fake the $W \to q\bar{q}$ decay.[9] To reduce this 'fake' background, it has been proposed[10] to make use of the quark jets naturally present in the $qq \to qqW^+W^-$ signal to 'tag' the event. The relevant QCD background is then $pp \to Wjjjj$, for which the exact matrix elements have only recently been computed.[11]

Existing studies[10] on quark jet tagging in Higgs production have been based on the s-channel approximation where only the Higgs exchange graph in $qq \to qqW^+W^-$ is taken into account. For $m_{WW} \gg m_H$, this approximation violates unitarity. However, for relatively small m_H (where Γ_H is also small), the approximation works well in the resonance region. On the other hand, for the range of m_H of interest at LHC and SSC energies, the Higgs width can be relatively large. In this case, there can be sizeable interference effects between the Higgs exchange graph and the non-resonant graphs which are not included in the approximation and which ultimately correct the unitarity violating behaviour. In this letter, we compute the exact matrix elements for $qq \to qqW^+W^-$ and use them to examine the jet tagging region. We make a detailed comparison with the s-channel approximation for the representative case $m_H = 800$ GeV and also determine the background contribution from the perturbative non-resonant graphs. Finally, we also compute the background contribution from the mixed electroweak-QCD processes, $gg \to q\bar{q}W^+W^-$, $qg \to qgW^+W^-$, $q\bar{q} \to ggW^+W^-$ and $qq \to qqW^+W^-$ in this region.

The $qq \to qqW^+W^-$ process receives contributions from W, Z, γ and gluon exchange in addition to Higgs exchange graphs leading to 130 Feynman diagrams in the unitary gauge for $uu \to uuW^+W^-$ and 104 Feynman diagrams for $ud \to udW^+W^-$. To compute the full matrix elements squared directly is a formidable task and, since the number of contributing Feynman diagrams depends on the quark flavours, not one to be recommended. As in Ref. 5, we use helicity techniques to compute helicity amplitudes for each Feynman diagram, which are then numerically summed and squared to obtain the full matrix elements. All interference effects and W decay correlations are then automatically evaluated. There are only six topologically distinct Feynman graphs (see Fig. 1 of Ref. 5), and, it is straightforward to

combine the helicity subamplitudes given in Ref. 5 with the appropriate coupling factors to give the full matrix element. Finally, we checked numerically that in the unbroken $SU(2) \times U(1)$ limit, the matrix elements are invariant under gauge transformations of the $W^{\pm}$ fields.

We have compared our results with the purely numerical results for the m_{WW} distribution given in Ref. 6. At small m_{WW}, we find good agreement, however, for $m_{WW} \gg m_H$, we find a somewhat smaller result. The discrepancy can be traced to the behaviour of the cross section for longitudinally polarised W's for intermediate photons and Z bosons at large m_{WW} in Ref. 6. This behaviour (see, for example, the dashed line in Fig. 10 of Ref. 6) seems to indicate that unitarity is violated and we have not managed to reproduce it.

Throughout this letter we use the following standard model parameters, $m_t = 120$ GeV, $\alpha = \alpha(M_Z) = 1/128$, $m_Z = 91.1$ GeV, $\sin^2\theta_W = 0.23$ and $M_W = M_Z \cos\theta_W = 80$ GeV. With these input parameters, the width of an 800 GeV Higgs boson is given by $\Gamma_H = 258.8$ GeV. Furthermore, we use the parton distributions of Duke and Owens (set 1)[12] evaluated at momentum scale $Q^2 = \hat{s}/4$. Since we are probing the hadron structure functions at large x there is little dependence on the choice of input parton distributions or on the choice of Q^2.

Figure 1 shows the W^+W^- invariant mass distribution, $d\sigma/dm_{WW}$, for $pp \to W^+W^-X$ at (a) the LHC and (b) the SSC for the representative Higgs boson mass, $m_H = 800$ GeV. Our principle interest is in the forward jet characteristics of W^+W^-jj events so we remain at the level of the W bosons and impose the rapidity cut, $|y_W| < 2.5$, on the W bosons. Since about 80% of the W decay products lie within 0.5 units of the parent W rapidity, this cut approximately simulates the coverage of the central electromagnetic and hadronic calorimeters of future hadron supercollider experiments. We also impose a separation in rapidity-azimuth of $\Delta R_{jj} > 0.7$ on the two jets in $qq \to qqW^+W^-$ and a transverse momentum cut of $p_{Tj} > 1$ GeV. These cuts regulate the collinear poles introduced by photon bremstrahlung diagrams,[5] and by $qq \to qq\gamma\gamma \to qqWW$ and $qq \to qqZ\gamma \to qqWW$ graphs. The total $qq \to qqW^+W^-$ cross section is stable under variation of these cuts.

The effect of the Higgs boson is evident as a resonance structure in the full calculation (solid curve) while the perturbative non-resonant background (dashed line) is smoothly falling. This background is obtained by evaluating the exact $qq \to qqW^+W^-$ matrix elements with $m_H \sim 0$. The unitarity violating contributions arising in both Higgs and non-Higgs graphs then cancel completely leaving a unitarity respecting distribution. Compared to the $qq \to qqZZ$ case,[8] the perturbative non-resonant background is relatively more important. This is because, in addition to the vector boson scattering processes, $qq \to qqWW \to qqWW$ and $qq \to qqZZ \to qqWW$, there are contributions from photon exchange processes, $qq \to qqZ\gamma \to qqWW$ and $qq \to qq\gamma\gamma \to qqWW$, which do not involve the Higgs boson and contribute only to the perturbative background.

We also find that the $q\bar{q} \to W^+W^-$ background is relatively more important than in the ZZ case. This is because of the large coupling of the W with quarks. On the other hand, apart from in the resonance region, the $qq \to qqW^+W^-$ process is dominated by Z and γ exchange and is relatively suppressed. Nevertheless, the perturbative non-resonant background represents a 30% (10%) correction to the $q\bar{q} \to W^+W^-$ rate in the resonance region at the SSC (LHC) and becomes even more important at larger values of m_{WW}. These corrections are thus of the same order of magnitude as one expects for the QCD corrections to $q\bar{q} \to W^+W^-$.[13]

The Higgs resonance is relatively more apparent at the SSC than at the LHC. In the resonance region, $m_H - \Gamma_H \leq m_{WW} \leq m_H + \Gamma_H$, the $qq \to qqW^+W^-$ cross section is 1.44 pb (0.24 pb) in the presence of the Higgs boson, while the perturbative non-resonant contribution is 0.82 pb (0.16 pb) at the SSC (LHC). The s-channel Higgs approximation yields 0.61 pb (0.08 pb) in the same region and accounts well for the difference in cross section due to the Higgs boson. Nevertheless, at larger m_{WW}, the s-channel approximation exceeds the full electroweak result due to its unitarity violating behaviour. We also see that the perturbative non-resonant background accounts for about 57% (67%) of the cross section in the resonance region.

The basic idea in jet tagging is to identify the additional quark jets present in $qq \to qqW^+W^-$ to enhance the Higgs boson signal relative to the backgrounds.

Although the perturbative non-resonant background still contributes, the relevant QCD background is, for example, $gg \to q\bar{q}W^+W^-$, which is suppressed by two powers of α_s relative to $q\bar{q} \to W^+W^-$. Similarly, in the semileptonic decay channel, $WW \to \ell\nu jj$, the QCD background is $W + 4$ jets rather than $W + 2$ jets.

To obtain some insight into the characteristics of the jets in $qq \to qqW^+W^-$, in Fig. 2 we show the higher and lower jet pseudorapidity distributions, $d\sigma/d|\eta_j|^{Hi}$ and $d\sigma/d|\eta_j|^{Lo}$, for our illustrative case of $m_H = 800$ GeV at the SSC. To emphasize the region of interest, we restrict m_{WW} to the resonance region, $m_H - \Gamma_H \leq m_{WW} \leq m_H + \Gamma_H$. Furthermore, in order to observe a jet, we impose a transverse momentum cut, $p_{Tj} > 50$ GeV, and a W-jet separation cut, $\Delta R_{Wj} > 0.7$, in addition to the jet-jet separation cut of $\Delta R_{jj} > 0.7$ mentioned earlier. At large m_{WW}, the W decay products tend to follow the direction of flight of the parent W boson so that the ΔR_{Wj} cut approximately corresponds to a separation cut between the W decay products and the jet of the same magnitude. The most significant cut for the $qq \to qqW^+W^-$ process is the transverse momentum cut which reduces the total $qq \to qqW^+W^-$ cross section in the resonance region to 0.64 pb (0.092 pb) at the SSC (LHC). The s-channel approximation contribution is more affected by the jet p_T cut and is reduced to 0.24 pb (0.025 pb) compared to 0.41 pb (0.065 pb) for the perturbative non-resonant background.

From Fig. 2a, we observe that the $|\eta_j|^{Hi}$ distribution for the full electroweak result (solid line) peaks around $|\eta_j|^{Hi} \sim 3.5$, while there is a separation between the s-channel Higgs approximation (dotted line) and the perturbative non-resonant background (dashed line) which peak at $|\eta_j|^{Hi} \sim 3.8$ and $|\eta_j|^{Hi} \sim 3.0$ respectively. On the other hand, the $|\eta_j|^{Lo}$ distribution is much flatter, peaking around $|\eta_j|^{Lo} \sim 2.6$ for the full result (solid curve). Once again, the perturbative non-resonant background is more important at smaller $|\eta_j|^{Lo}$, while the s-channel Higgs approximation gives the larger contribution at large $|\eta_j|^{Lo}$. In order to preserve as much of the signal as possible, Fig. 2 suggests a jet tagging region of $2.5 < |\eta_j| < 5.0$ is appropriate at the SSC. Nevertheless, this region still receives a sizeable contribution from the perturbative non-resonant background – 0.08 pb (0.008 pb) compared to 0.18 pb (0.017 pb) in the presence of the Higgs boson at the SSC (LHC). The s-channel approximation again correctly estimates the signal cross section in the

tagging region – 0.10 pb (0.009 pb). It is also clear that reducing the upper rapidity cut from 5.0 to 4.5 has a smaller effect on the signal than increasing the lower cut from 2.5 to 3.0.

We also show the contribution from the mixed QCD-electroweak $pp \to W^+W^-jj$ processes. The $gg \to q\bar{q}W^+W^-$ process receives contributions from 23 Feynman diagrams in the unitary gauge and we have made use of the helicity subamplitudes presented in Ref. 5 to compute the full matrix elements. In addition to the three diagram topologies shown in Fig. 2 of Ref. 5, there is a contribution from graphs containing both a triple gluon vertex and a triple electroweak boson vertex, resulting in one new helicity subamplitude. We have checked that the matrix elements are invariant under gauge transformations of the gluon fields and, in the appropriate limit, of the $W^\pm$ fields. Furthermore, we have reproduced the numerical results of Ref. 14. The infrared and collinear divergences inherent in the mixed QCD-electroweak amplitudes are regulated by the p_{Tj} and ΔR_{jj} cuts. However, relatively large logarithms, for example, $\log(m_H^2/p_{Tj}^2) \sim 5.5$, can still occur and which tend to reduce the naive α_s^2 suppression relative to the lowest order $q\bar{q} \to W^+W^-$ process. The QCD cross section is still quite large, 2.7 pb, however, as shown in Fig. 2, it is peaked at small rapidities. Once the jet pseudorapidity is restricted to the tagging region, the QCD background is reduced by a factor of around 50 to 0.06 pb, approximately one third of the full electroweak cross section in this region.

The $|\eta_j|^{Lo}$ and $|\eta_j|^{Hi}$ distributions for the LHC are rather similar to those shown in Fig. 2. The signal peaks at slightly smaller $|\eta_j|^{Hi}$ and $|\eta_j|^{Lo}$, however, due to the dominance of the QCD background at small $|\eta_j|$, a lower bound on the jet pseudorapidity of $|\eta_j| > 2.5$ is advisable for the jet tagging region. In this case almost no cross section occurs beyond $|\eta_j| = 4.5$, so that the rapidity coverage of the forward detector can be reduced to $2.5 < |\eta_j| < 4.5$.

As mentioned earlier, the jet p_T cut reduces the cross section from Higgs boson events appreciably. However, in order to cleanly define a jet in the forward region and to reduce the contamination when the underlying event 'fakes' the tagging jet, it may be necessary to increase the jet p_T cut. To illustrate the effect of increasing

the jet p_T cut, we show the smaller of the two jet transverse momenta, p_{Tj}^{Lo}, in Fig. 3. Increasing the jet p_T cut is equivalent to moving to larger p_{Tj}^{Lo}. We focus on the resonance region of an 800 GeV Higgs boson at the SSC and restrict the jet pseudorapidity to the forward region, $2.5 < |\eta_j| < 5.0$. Fig. 3 shows that at small p_{Tj}^{Lo}, the major part of the full electroweak result (solid) line comes from $qq \to qqH \to qqW^+W^-$ events (dotted line). This is not surprising since each jet typically has p_T of order M_W. With increasing p_{Tj}^{Lo}, the Higgs contribution rapidly diminishes and the perturbative non-resonant contribution becomes more important, eventually dominating for $p_{Tj}^{Lo} > 200$ GeV. The QCD background (dash-dotted line) has a similar behaviour to the full electroweak result, but is smaller by about a factor of 3 – 4. Clearly increasing the jet p_T cut not only reduces the signal cross section, but also worsens the signal to electroweak background ratio which becomes less than 1 to 1 for $p_{Tj} \geq 100$ GeV.

Finally, in Fig. 4, we show the m_{WW} distribution for WW events containing two tagged jets. Compared to the untagged case (see Fig. 1), the Higgs resonance structure for the full electroweak result (solid line) is somewhat sharpened, although the peak height in the resonance region has fallen by a factor of 8 (10) at the SSC (LHC). Even so, if the large semileptonic WW branching ratio can be utilised, a significant number of signal events remain in the resonance region. Furthermore, the perturbative non-resonant contribution at the peak has been reduced to 25% (19%) compared to a 40% (47%) effect in the no-tag case at the SSC (LHC).

The s-channel Higgs exchange contribution (dotted line) shows its unitarity violating behaviour at much smaller m_{WW}, exceeding the full result at $m_{WW} \sim$ 850 GeV (900 GeV) at the SSC (LHC). To emphasize how bad the approximation is at reproducing the invariant mass distribution of the signal, we also show the difference, Δ, between the exact result in the presence of the Higgs boson and the perturbative non-resonant background in the resonance region (long-dashed line). The approximation significantly underestimates the true signal for $m_{WW} < m_H$ and overshoots for $m_{WW} > m_H$. Although the peak heights are approximately equal, the approximation peaks at higher m_{WW}. Nevertheless, within the resonance region, the s-channel approximation (accidentally) accounts reasonably well for the difference in cross section between the full result and the perturbative non-resonant

background.

By tagging on both jets, the large $q\bar{q} \to W^+W^-$ background has been reduced in the peak region by a factor of around 70 reflecting the two additional powers of α_s required to form the two tagged jets. We also see that the QCD $WWjj$ background falls much faster than the electroweak cross section, and gives a relatively small contribution of 14% (9%) in the peak region at the SSC (LHC), which is even smaller than the perturbative non-resonant background. On the other hand, when integrated over the resonance region, $m_H - \Gamma_H < m_{WW} < m_H + \Gamma_H$, the QCD and perturbative non-resonant backgrounds give contributions of 0.06 pb (0.015 pb) and 0.08 pb (0.008 pb) respectively at the SSC (LHC) which is to be compared with the signal cross section of 0.10 pb (0.009 pb).

In summary, we have presented the results of a complete perturbative calculation of W^+W^- pair production via the tree level $\mathcal{O}(\alpha_W^4)$ electroweak $qq \to qqW^+W^-$ process, focussing on the identification of jets in the forward region. Previous studies[10] have been based on the unitarity violating s-channel Higgs approximation. For jet tagging, there are two important parameters, the allowed jet pseudorapidity region and the jet p_T (or equivalently jet energy) cut. To preserve as much of the signal as possible, the optimal jet tagging region appears to be $2.5 < |\eta_j| < 5.0$ at the SSC and $2.5 < |\eta_j| < 4.5$ at the LHC. We have assumed that jet identification is possible provided the jet p_T is larger than 50 GeV (which corresponds to a jet energy cut of 300 GeV). However, if larger jet p_T's are required to cleanly identify the jet, the Higgs signal is reduced relative to the perturbative non-resonant background. For our illustrative example, $m_H = 800$ GeV, we find that by requiring that both jets are 'tagged', the Higgs signal is enhanced relative to the perturbative non-resonant background – the minimal electroweak contribution – and relative to mixed QCD-electroweak W^+W^-jj production. Although the s-channel Higgs approximation appears to predict the signal cross section in the resonance region reasonably accurately, it does not produce the correct m_{WW} behaviour.

Our conclusions are based on a purely parton level study and are incomplete in several respects. Throughout we have concentrated on the central production of

W^+W^- pairs without regard to their decay. In fact, to enable a clean separation between the central W decay products and the tagged jets, it may be necessary to further restrict the W rapidity range to, for example, $|y_W| < 1.5$. In this case, the tagging jet distributions are essentially unaffected in shape while the normalisation is reduced by approximately 55%. Furthermore, once the W decays, it is impossible to reconstruct the WW invariant mass unambiguously. Nevertheless, the basic conclusion that tagging enhances the signal remains unaltered.

Finally, we have not studied the additional background arising from top quark production, $q\bar{q}, gg \to t\bar{t} \to W^+W^-b\bar{b}$, and, in the case when one W decays hadronically, fake QCD backgrounds such as, $pp \to Wjjjj$. Both of these backgrounds are potentially overwhelming and deserve further study, as are the effects of hadronisation and leakage from the underlying event.

ACKNOWLEDGEMENTS

We thank K. Einsweiler, D. Froidevaux, W. Giele and C. P. Yuan for fruitful discussions. This research was supported in part by the University of Wisconsin Research Committee with funds granted by the Wisconsin Alumni Research Foundation, by the U. S. Department of Energy under contract DE-AC02-76ER00881, and by awards granted by the Texas National Research Laboratory Commission.

REFERENCES

1. H. Georgi, S. L. Glashow, M. E. Mahacek and D. V. Nanopoulos, Phys. Rev. Lett. **40**, 692 (1978).
2. D. A. Dicus, C. Kao and W. W. Repko, Phys. Rev. **D36**, 1570 (1987).
3. E. W. N. Glover and J. J. van der Bij, Phys. Lett. **219B**, 488 (1989), and Nucl. Phys. **B321**, 561 (1989).
4. D. A. Dicus, S. L. Wilson and R. Vega, Phys. Lett. **192B**, 231 (1987).
5. U. Baur and E. W. N. Glover, FERMILAB-PUB-90/75-T, MAD/PH/562, preprint (April 1990), to appear in Nucl. Phys. **B**.
6. D. A. Dicus and R. Vega, Phys. Rev. **D37**, 2474 (1988).
7. K. Sliwa, talk given at the XXVth Recontres de Moriond, Les Arcs, France, March 4 – 18, 1990, FERMILAB-Conf-90/93-E (preprint), and references therein.
8. U. Baur and E. W. N. Glover, FERMILAB-PUB-90/154-T, MAD/PH/577, preprint (August 1990), submitted to Phys. Rev. **D**.
9. S. D. Ellis, R. Kleiss and W. J. Stirling, Phys. Lett. **163B**, 261 (1985);
   J. F. Gunion, Z. Kunszt and M. Soldate, Phys. Lett. **163B**, 389 (1985).
10. R. N. Cahn, S. D. Ellis, R. Kleiss and W. J. Stirling, Phys. Rev. **D35**, 1626 (1987);
    R. Kleiss and W. J. Stirling, Phys. Lett. **200B**, 193 (1988):
    W. J. Stirling, CERN 88-02 report (1988) ed. J. H. Mulvey, p. 73.
11. W. Giele, private communication;
    F. A. Berends, W. T. Giele, H. Kuijf and B. Tausk, in preparation.
12. D. Duke and J. Owens, Phys. Rev. **D30**, 49 (1984).
13. V. Barger, J. L. Lopez and W. Putikka, Int. J. Mod. Phys. **A3**, 2181 (1988).
14. V. Barger, T. Han, J. Ohnemus and D. Zeppenfeld, Phys. Rev. **D41**, 2782 (1990).

FIGURE CAPTIONS

1. Invariant mass distribution, $d\sigma/dm_{WW}$, of the W boson pair in $pp \to W^+W^-X$ at (a) the LHC and (b) the SSC. The solid line shows the $qq \to qqW^+W^-$ result for $m_H = 800$ GeV. The $m_H = 0$ curve (dashed line) represents the perturbative non-resonant $qq \to qqW^+W^-$ background. The dotted line gives the result obtained with the s-channel Higgs pole approximation, while the dash-dotted curve shows the continuum $q\bar{q} \to W^+W^-$ cross section. Both W bosons are required to have rapidity, $|y_W| < 2.5$. A $p_{Tj} > 1$ GeV cut and a $\Delta R_{jj} > 0.7$ separation cut are imposed in $qq \to qqW^+W^-$.

2. Distributions of (a) the maximum and (b) the minimum jet pseudorapidity, $|\eta_j|^{Hi}$ and $|\eta_j|^{Lo}$, in $pp \to W^+W^-jj$ for $p_{Tj} > 50$ GeV and $m_H = 800$ GeV at the SSC in the Higgs resonance region, $m_H - \Gamma_H < m_{WW} < m_H + \Gamma_H$. The solid line shows the exact result from $qq \to qqW^+W^-$. The dotted curve represents the result in the Higgs pole approximation, while the dashed line gives the perturbative background from the non-resonant electroweak $qq \to qqW^+W^-$ diagrams. The dash-dotted curve, finally, shows the result from mixed QCD-electroweak diagrams. Both W bosons are required to have rapidity , $|y_W| < 2.5$, and a jet-jet and W-jet separation cut of ΔR_{jj}, $\Delta R_{Wj} > 0.7$ is imposed.

3. Distribution of the minimum transverse momentum, p_{Tj}^{Lo}, in $pp \to W^+W^-jj$ for $2.5 < |\eta_j| < 5.0$ and $m_H = 800$ GeV at the SSC in the Higgs resonance region, $m_H - \Gamma_H < m_{WW} < m_H + \Gamma_H$. The solid line shows the exact result from $qq \to qqW^+W^-$. The dotted curve represents the result in the Higgs pole approximation, while the dashed line gives the perturbative background from the non-resonant electroweak $qq \to qqW^+W^-$ diagrams. The dash-dotted curve, finally, shows the result from mixed QCD-electroweak diagrams. Both W bosons are required to have rapidity , $|y_W| < 2.5$, and a jet-jet and W-jet separation cut of ΔR_{jj}, $\Delta R_{Wj} > 0.7$ is imposed.

4. Invariant mass distribution, of the W boson pair in $pp \to W^+W^-jj$ at (a) the LHC and (b) the SSC in the jet tagging region. The solid line shows the $qq \to qqW^+W^-$ result for $m_H = 800$ GeV. The $m_H = 0$ curve (dashed

line) represents the perturbative non-resonant $qq \to qqW^+W^-$ background. The dotted line gives the result obtained with the s-channel Higgs pole approximation, while the dash-dotted curve shows the background from mixed QCD-electroweak processes. The long dashed curve, Δ, shows the difference between the full electroweak result and the perturbative non-resonant background. Both W bosons are required to have rapidity, $|y_W| < 2.5$, and a $\Delta R_{jj},\ \Delta R_{Wj} > 0.7$ separation cut is imposed.

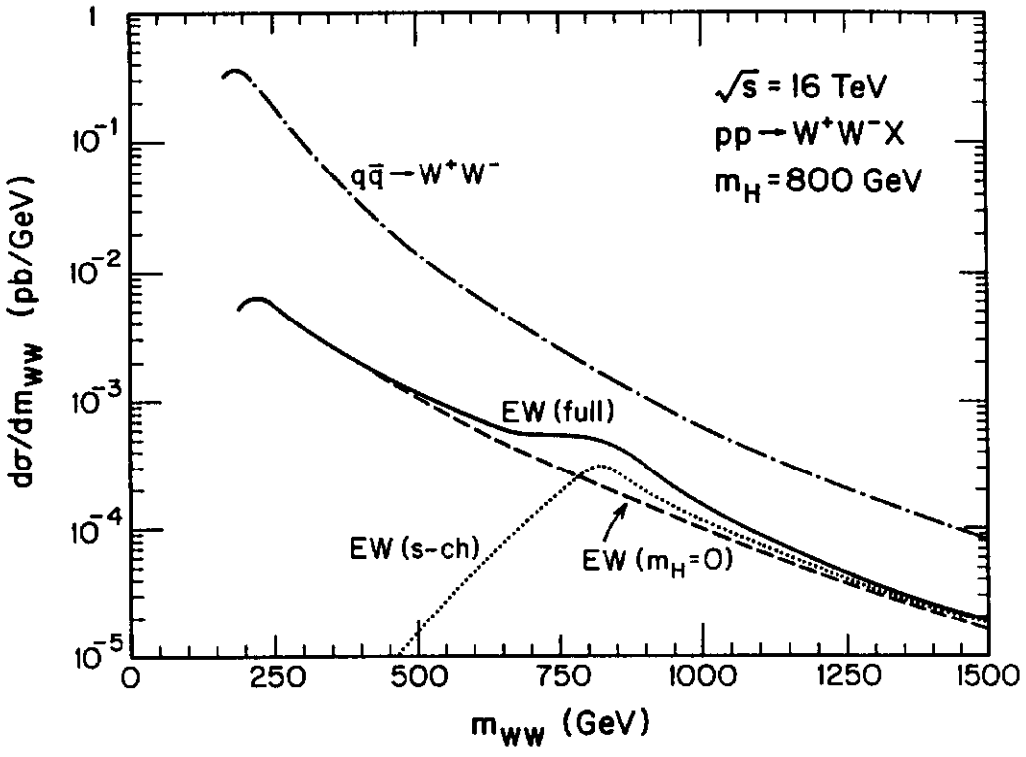
√s = 16 TeV
pp → W⁺W⁻X
m_H = 800 GeV
qq̄ → W⁺W⁻
EW (full)
EW (s-ch)
EW (m_H=0)
dσ/dm_WW (pb/GeV)
m_WW (GeV)
1
10⁻¹
10⁻²
10⁻³
10⁻⁴
10⁻⁵
0
250
500
750
1000
1250
1500

Fig. 1a

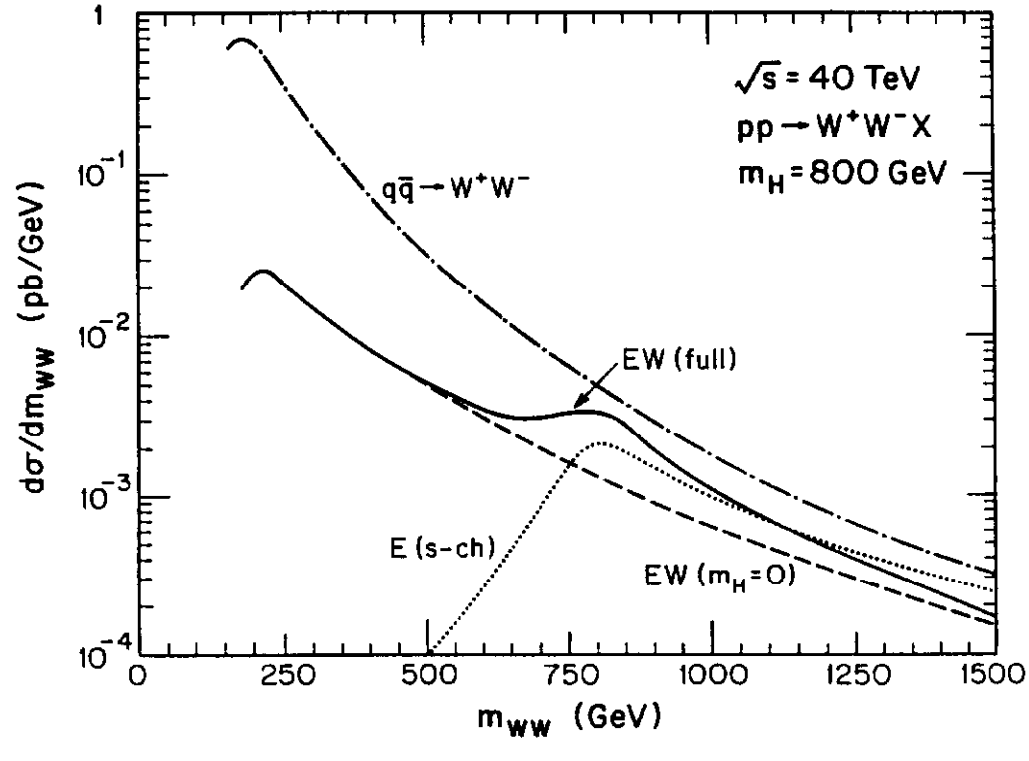
√s = 40 TeV
pp → W⁺W⁻X
m_H = 800 GeV
qq̄ → W⁺W⁻
EW (full)
E (s-ch)
EW (m_H=0)
dσ/dm_WW (pb/GeV)
m_WW (GeV)
1
10⁻¹
10⁻²
10⁻³
10⁻⁴
0
250
500
750
1000
1250
1500

Fig. 1b

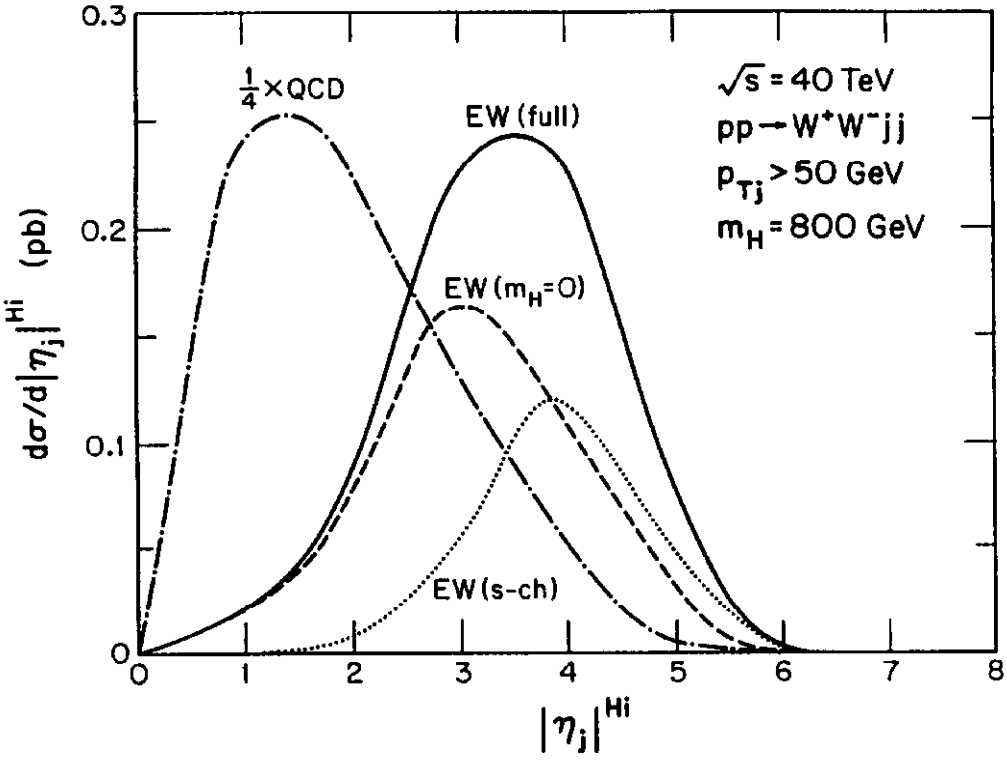
0.3
0.2
0.1
0
0
1
2
3
4
5
6
7
8
$\frac{1}{4}\times$QCD
EW (full)
EW (m_H=0)
EW (s-ch)
$\sqrt{s}$ = 40 TeV
$pp \rightarrow W^+W^-jj$
$p_{Tj} > 50$ GeV
m_H = 800 GeV
$d\sigma/d|\eta_j|^{Hi}$ (pb)
$|\eta_j|^{Hi}$

Fig. 2a

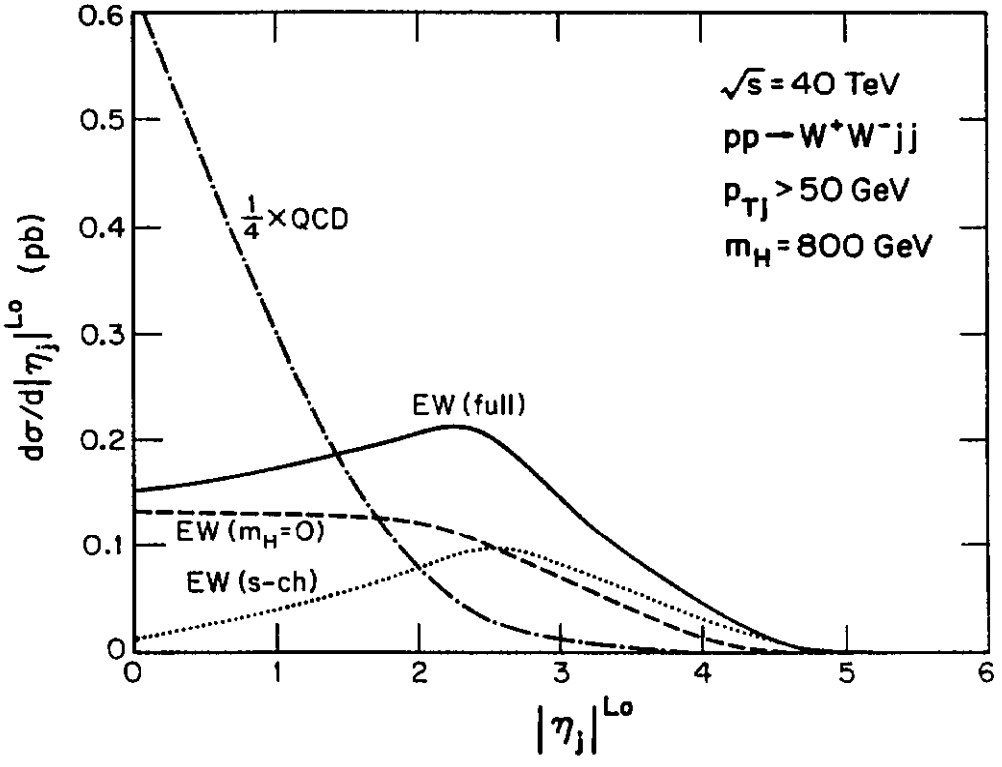
0.6
0.5
0.4
0.3
0.2
0.1
0
0
1
2
3
4
5
6
$\frac{1}{4}\times$QCD
EW (full)
EW (m_H=0)
EW (s-ch)
$\sqrt{s}$ = 40 TeV
$pp \rightarrow W^+W^-jj$
$p_{Tj} > 50$ GeV
m_H = 800 GeV
$d\sigma/d|\eta_j|^{Lo}$ (pb)
$|\eta_j|^{Lo}$

Fig. 2b

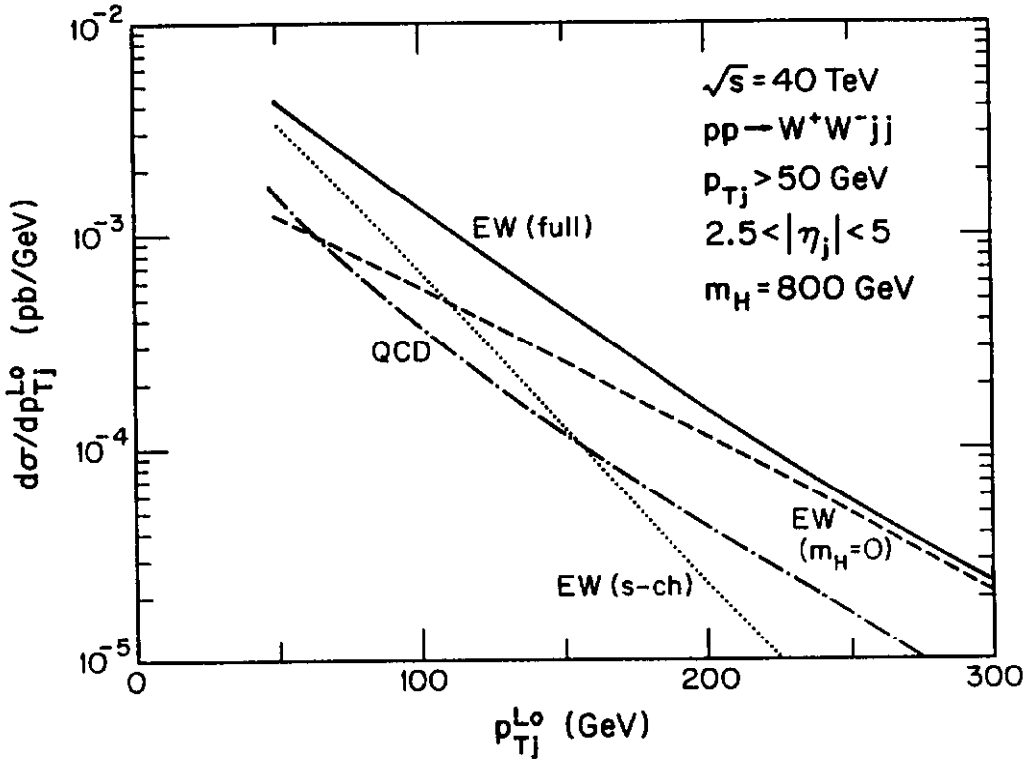
10^{-2}
10^{-3}
10^{-4}
10^{-5}
$d\sigma/dp_{Tj}^{Lo}$ (pb/GeV)
0
100
200
300
p_{Tj}^{Lo} (GeV)
$\sqrt{s}$ = 40 TeV
$pp \to W^+W^-jj$
$p_{Tj} > 50$ GeV
$2.5 < |\eta_j| < 5$
m_H = 800 GeV
EW (full)
QCD
EW
(m_H=0)
EW (s-ch)

Fig. 3

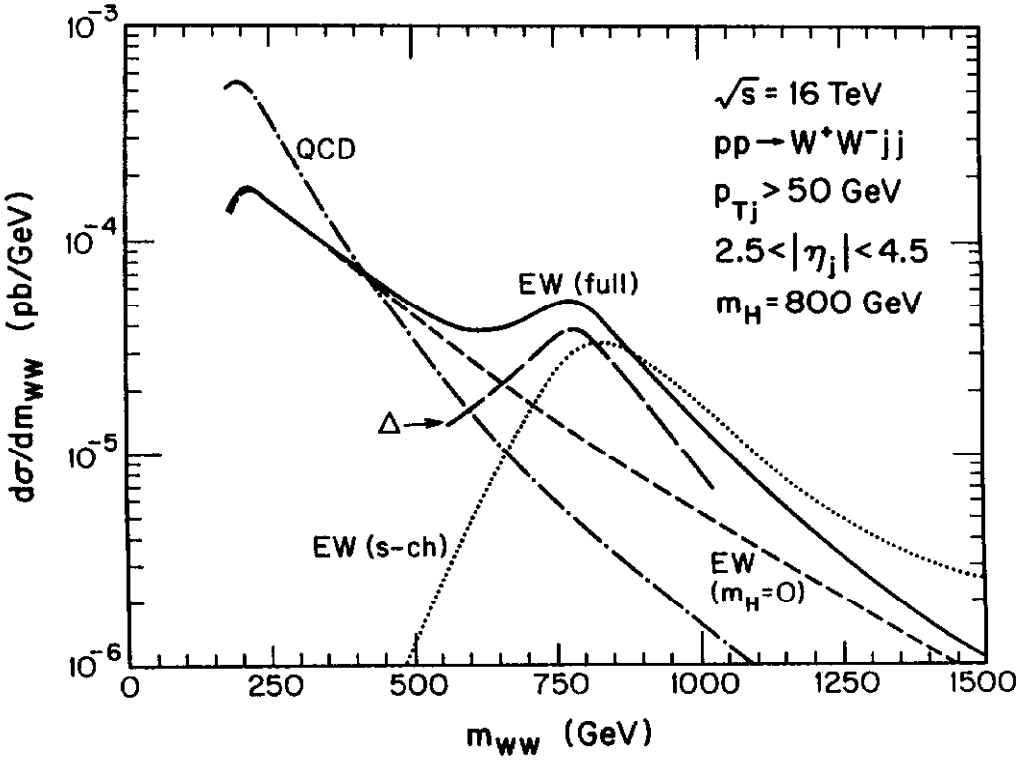
$\sqrt{s}$ = 16 TeV
pp → W⁺W⁻jj
p_{Tj} > 50 GeV
2.5 < |η_j| < 4.5
m_H = 800 GeV
QCD
EW (full)
EW (s-ch)
EW (m_H=0)
Δ
$d\sigma/dm_{WW}$ (pb/GeV)
m_{WW} (GeV)
10^{-3}
10^{-4}
10^{-5}
10^{-6}
0
250
500
750
1000
1250
1500

Fig. 4a

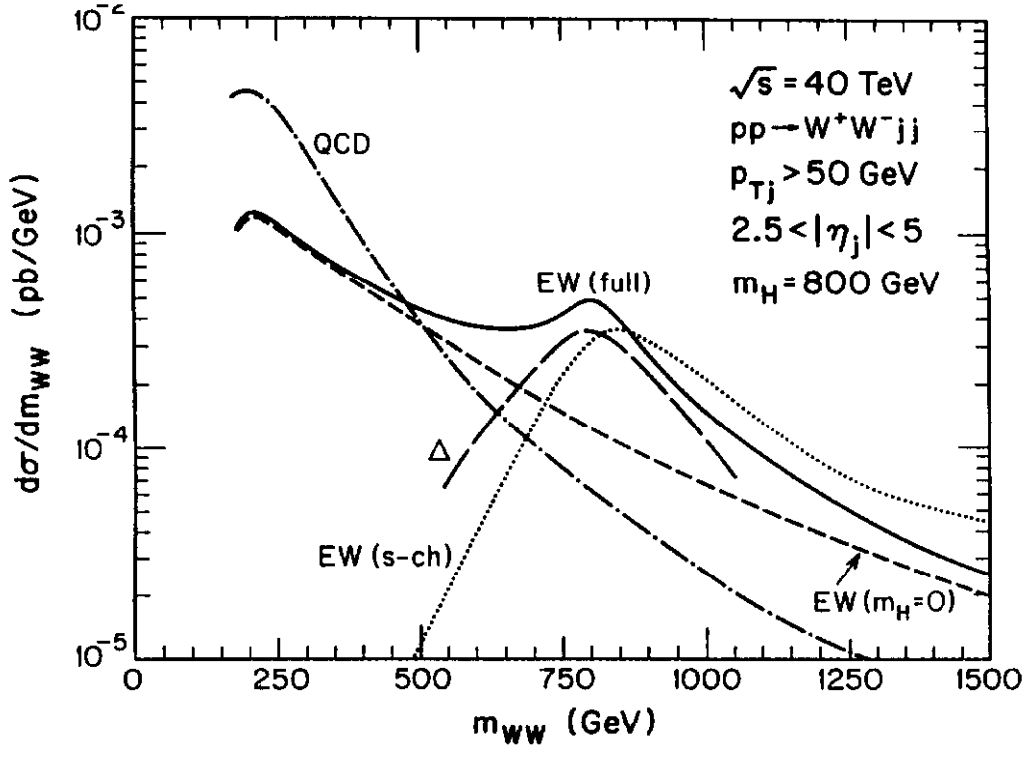
$\sqrt{s}$ = 40 TeV
pp → W⁺W⁻jj
p_{Tj} > 50 GeV
2.5 < |η_j| < 5
m_H = 800 GeV
QCD
EW (full)
EW (s-ch)
EW (m_H=0)
Δ
$d\sigma/dm_{WW}$ (pb/GeV)
m_{WW} (GeV)
10^{-3}
10^{-4}
10^{-5}
0
250
500
750
1000
1250
1500

Fig. 4b